Jpn. J. Appl. Phys. Vol. 34 (1995) pp. 4977–4982
Part 1, No. 9A, September 1995

Electron Distribution Functions in a Sputtering Magnetron Discharge

T. E. SHERIDAN*[1,*2], M. J. GOECKNER*[3,*4] and J. GOREE
Department of Physics and Astronomy, The University of Iowa, Iowa City, Iowa 52242, The United States of America

(Received January 19, 1995; accepted for publication June 15, 1995)

The electron distribution function $g(v_z)$ in a cylindrically symmetric, planar, sputtering magnetron has been characterized using a one-sided, planar Langmuir probe. Measurements were made above the magnetic trap at six radial locations in the direction normal to the cathode. The distribution function is found to be non-Maxwellian, with a shape that depends sensitively on radial position. Near the symmetry axis, $g(v_z)$ is anisotropic and exhibits a strong electron drift from the cathode to the anode. Off axis, $g(v_z)$ is nearly symmetric and has two components: a dense, cold Maxwellian component, and a tenuous, energetic shell component.

KEYWORDS: sputtering magnetron, plasma, electron distribution function, Langmuir probe

1. Introduction

Sputtering magnetrons[1,2] are employed both for thin film deposition and sputter etching. In these devices a magnetic trap is used to confine electrons near a negatively-biased cathode, creating an intense, localized source of ionization above that cathode.[3,4] Ions created in the magnetic trap impact the cathode with several hundred electron volts of energy, sputtering material from the cathode and liberating secondary electrons. The secondary electrons are accelerated through the sheath into the trap region, thus sustaining the discharge.

Because of their commercial importance, developing an understanding of sputtering magnetron physics has attracted continuing interest. On the theoretical side, a Monte Carlo model[4–7] of electron transport has been developed that accurately predicts the etch track profile and therefore target utilization. This model has also been used to investigate the influence of neutral pressure[8] and magnetic field strength[9] on magnetron operation. On the experimental side, Langmuir probe,[10–13] laser-induced fluorescence,[14,15] and optical emission diagnostics[16,17] have all been used to characterize the magnetron plasma.

Much of our experimental understanding of magnetron operation comes from cylindrical Langmuir probe measurements.[10–13] It has been noted that the probe's current-voltage characteristic sometimes appears to be non-Maxwellian.[10] For example, we have analyzed probe characteristics using a two-temperature model[18] and found cold, dense and hot, tenuous electron populations outside the trap region. That the distribution function is non-Maxwellian is not unexpected, as the source is localized to the magnetic trap region and the neutral pressure is low enough so that the electron mean free path is relatively long. Additionally, there are strong $\boldsymbol{E}\times\boldsymbol{B}$ electron drifts in the trap region,[19] and there must be electron transport from the trap region to the anode to balance the ion current to the cathode.[20] Unfortunately, cylindrical probes are inappropriate for exploring the details of the electron distribution function as they average over a cylindrical volume. For example, it has been shown[21] that if the electron drift is not properly accounted for, erroneously low plasma potentials and high electron temperatures will be inferred from the probe characteristic.

In this paper, we use a one-sided planar Langmuir probe to make what we believe are the first detailed measurements of the electron distribution function in a sputtering magnetron discharge. We find that the electron distribution function is non-Maxwellian and anisotropic. The anisotropy is due to the flow of electrons from the magnetic trap to the anode. These measurements provide direct verification of the electron transport from the magnetic trap to the anode seen in Monte Carlo simulations.[4,5,9] Further, at large radii the electron distribution function has two populations: a cold, Maxwellian component and an energetic, shell component.

In §2 we explain how the electron distribution function is obtained from the current-voltage characteristic of a planar probe. In §3 the sputtering magnetron and planar probe used are described, in §4 our results are presented and interpreted, and §5 contains our conclusions.

2. Planar Probe Theory

Here we review the theory appropriate for recovering the reduced electron distribution function $g(v_z)$ from two, one-sided planar probe characteristics.[22] The distribution function is not assumed to be isotropic.

Take the normal to the probe face to be in the negative z-direction, so that electrons with a positive z-component of velocity $v_z>0$ travel towards the probe face. To be collected by the probe, an electron must have enough energy to overcome the potential barrier at the probe and must be going toward the probe. Thus, we require $\frac{1}{2}mv_z^2 \geq eV_{\text{probe}}$, and $v_z>0$, where m is the electron mass, e is the electron charge, and V_{probe} is the negative probe bias measured with respect to the plasma potential V_{p}. The z-component of the electron current density $J_{z,\text{probe}}$ at the probe face is given by an integral over

*[1]Present address: *Department of Physics, West Virginia University, Morgantown, West a Virginia 26506-6315, The United States of America.*
*[2]E-mail address: tesheri@wvnvms.wvnet.edu
*[3]Present address: *Princeton University, Plasma Physics Laboratory, James Forrestal Campus, Post Office Box 451, Princeton, New Jersey 08543, The United States of America.*
*[4]E-mail address: mgoeckner@pppl.gov

the electron distribution function $f(v_x, v_y, v_z)$:

$$J_{z,\text{probe}}=e\int_{-\infty}^{\infty}dv_x\int_{-\infty}^{\infty}dv_y\int_{\sqrt{2eV_{\text{probe}}/m}}^{\infty}dv_z v_z f(v_x, v_y, v_z), \tag{1}$$

where $f(v_x, v_y, v_z)$ is normalized so that its integral gives the electron density. As the distribution function is only measured for the z-direction, we reduce $f(v_x, v_y, v_z)$ by integrating over the velocity components normal to v_z (i.e., v_x and v_y). The reduced distribution function $g(v_z)$ is defined as

$$g(v_z)=\int_{-\infty}^{\infty}dv_x\int_{-\infty}^{\infty}dv_y f(v_x, v_y, v_z). \tag{2}$$

It is $g(v_z)$ that we measure experimentally. In terms of $g(v_z)$ the current density collected by the probe is

$$J_{z,\text{probe}}=e\int_{\sqrt{2eV_{\text{probe}}/m}}^{\infty}dv_z v_z g(v_z). \tag{3}$$

The reduced distribution function can be recovered from the collected electron current by differentiating $J_{z,\text{probe}}$ with respect to the probe bias V_{probe}, so that

$$g\left(v_z=\sqrt{\frac{2eV_{\text{probe}}}{m}}\right)=-\frac{m}{e^2}\frac{dJ_{z,\text{probe}}}{dV_{\text{probe}}}. \tag{4}$$

The entire reduced distribution function (i.e., v_z both positive and negative) is recovered by measuring $J_{z,\text{probe}}(V_{\text{probe}})$ with the probe facing in the negative and positive z-directions.

Once the reduced distribution function has been recovered from the probe characteristic, moments of the distribution function (*e.g.*, density and average velocity) can be computed. The electron density is the integral of $g(v_z)$ over all velocities

$$n=\int_{-\infty}^{\infty}dv_z g(v_z). \tag{5}$$

and the average z-velocity $\langle v_z\rangle$ is

$$\langle v_z\rangle=\frac{1}{n}\int_{-\infty}^{\infty}dv_z v_z g(v_z), \tag{6}$$

where the sign of $\langle v_z\rangle$ gives the direction of the net electron flow, and $\langle v_z\rangle=0$ for a symmetric distribution function. In calculating $\langle v_z\rangle$, $g\langle v_z\rangle$ is weighted by v_z, so that the details of the distribution function near $v_z=0$ are relatively unimportant. The electron current density J_z (not $J_{z,\text{probe}}$) can be computed from n and $\langle v_z\rangle$ by

$$J_z=en\langle v_z\rangle. \tag{7}$$

This is the net electron current density flowing "through" the probe. Using a cylindrical probe there is no way to measure J_z. Finally, the average of the velocity-squared $\langle v_z^2\rangle$ can be written as

$$\langle v_z^2\rangle=\frac{1}{n}\int_{-\infty}^{\infty}dv_z(v_z-\langle v_z\rangle)^2 g(v_z), \tag{8}$$

where $\langle v_z^2\rangle$ is a measure of the width of the distribution function. This quantity is related to the average electron energy E_{ave} by $E_{\text{ave}}=\frac{1}{2}m\langle v_z^2\rangle$. If the distribution function is Maxwellian then it can be characterized by a temperature T and $E_{\text{ave}}=\frac{1}{2}kT$. However, even if $g(v_z)$ is non-Maxwellian, we can still define an effective "temperature" T_{eff} for the distribution function by

$$T_{\text{eff}}=m\langle v_z^2\rangle/k \tag{9}$$

where T_{eff} is a measure of the average electron energy. If the distribution function is Maxwellian then $T_{\text{eff}}=T$.

3. Apparatus

The magnetron used for this experiment, which has been described in detail elsewhere,[9,12] is a cylindrically symmetric planar device with a 76.2-mm (3.0-inch) diameter copper cathode target. The magnetic field configuration is shown in Fig. 1, where z is the height above the cathode, and r is the radial distance from the cylindrical axis. The field is produced by permanent magnets, and has a value of 245 G on the cathode surface ($z=0$) at a radius $r=17$ mm. At this radius the magnetic field is tangential to the cathode. Empirically, the magnetic trap region is enclosed by field lines that both begin and end on the cathode. The magnetic configuration of our device is classified as a "type II unbalanced magnetron,"[23] so that the far-field dipole moment is dominated by the outer ring of magnets. Consequently, there are field lines connecting the cathode to the facing anode, as shown in Fig. 1. Electrons escape from the magnetic trap region when they are scattered onto field lines connected to the anode. Most escaping electrons are found at radii $r<20$ mm (see Fig. 7 in ref. 4) due to the magnetic field configuration.

To measure the electron distribution function we constructed a small, one-sided, planar probe with a 3.4-mm diameter circular copper face. To prevent shorting between the probe face and insulating probe body as

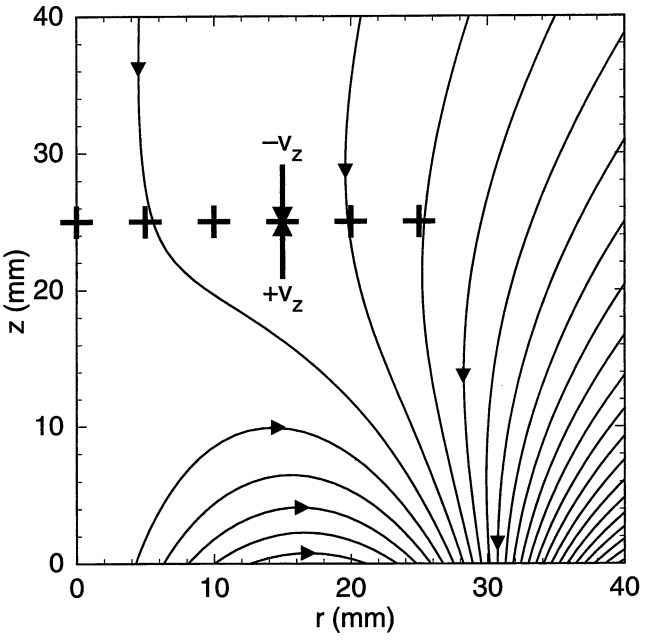

Fig. 1. Magnetic field configuration of the cylindrically symmetric sputtering magnetron used for this work. The cathode is at $z=0$, and a grounded, planar anode faces the cathode. Electrons with $v_z>0$ travel away from the cathode. Crosses at $z=25$ mm indicate locations where the electron distribution function was measured.

the probe was coated by sputtered copper from the cathode, the probe was built with a narrow gap between its face and body. Further, since the probe face was copper, its electron collection properties should not have changed much as it was coated by sputtered copper. From measured electron densities and temperatures, we find that the Debye length λ_D varied from ≈ 0.14 mm at $r=0$ mm to ≈ 0.09 mm for $r=25$ mm, so that the probe is at least 24 λ_D in diameter, assuring us that it does indeed act as a planar probe. Though this probe is small, it still causes a large reduction in the discharge current when placed in the magnetic trap region. Therefore, all measurements were made outside of the magnetic trap.

4. Results and Discussion

The magnetron was used with a copper cathode at a neutral pressure of 1.0 Pa argon. The cathode was biased to -400 V dc, giving a discharge current of 51 mA and an average current density at the cathode of ≈ 46 A/m^2. Probe characteristics were taken at a fixed height $z=25$ mm above the cathode and at radii $r=0$, 5, 10, 15, 20 and 25 mm with the probe facing toward and away from the cathode (the negative and positive z-directions), as shown in Fig. 1.

The probe characteristics measured at $r=5$ mm are shown in Fig. 2. The electron current collected when the probe faces the cathode is much greater than that collected when it faces the anode, indicating an electron drift from the cathode to the anode.[22] When the probe current is plotted on a logarithmic scale [Fig. 2(b)] we see that the electron current increases rapidly just below the knee of the characteristic, indicating an electron distribution function having two components with differing temperatures.[18]

The radial dependence of the plasma potential V_p is shown in Fig. 3 as a solid line. We take the plasma potential as the more positive of the inflection points for the two probe characteristics acquired at a given radius. For $r=0$, 5, and 10 mm there is a difference between the inflection points of the two characteristics with an average value of 0.13 V, indicating a net electron drift away from the cathode. For $r=15$, 20 and 25 mm the values of the inflection point agree to within 0.01 V at each radius. The plasma potential is ≈ 0.9 V on axis and rises to ≈ 1.15 V at larger radii. The depression in V_p on axis must be due to an excess of electrons over ions, and the small radial electric field acts to push these extra electrons to larger radii. Due to the large electron drifts at $r=0$, 5 and 10 mm the plasma potential inferred from cylindrical probe characteristics may underestimate the true plasma potential.[21]

Reduced distribution functions were calculated from the probe characteristics as follows. As the ion current depends only weakly on the probe bias for a planar probe, we assume that any contribution to the derivative [eq. (4)] from the ions is much, much smaller than that from the electrons, and compute $g(v_z)$ from the total current collected by the probe. Due to the paucity of data points near zero velocity [because of the square root in eq. (4)], the distribution function around $v_z=0$ is

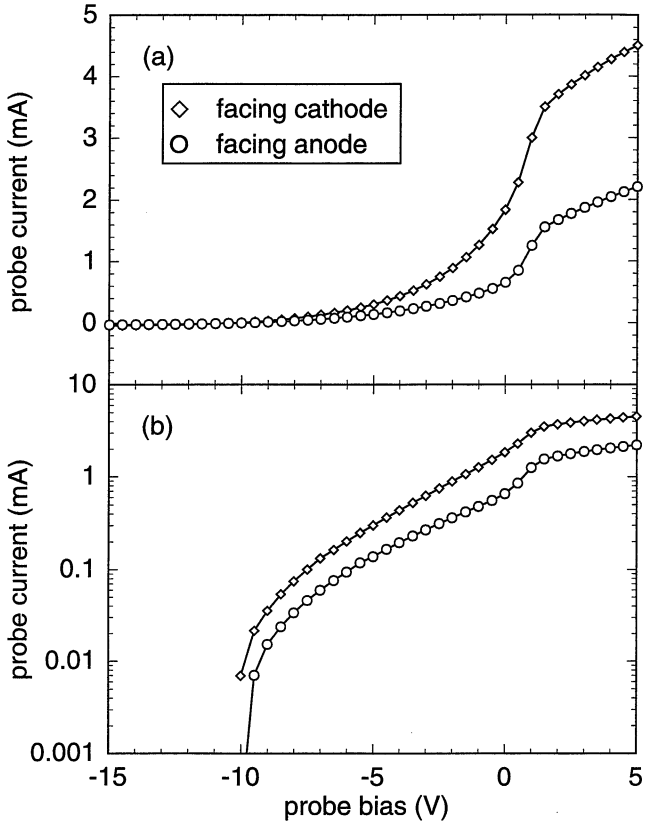

Fig. 2. Planar probe characteristics taken at $r=5$ mm plotted on (a) linear axes and (b) semilogarithmic axes. Note the strong asymmetry between the characteristic taken facing the cathode and that taken facing the anode. The electron current flowing away from the cathode is much greater than the current flowing toward it.

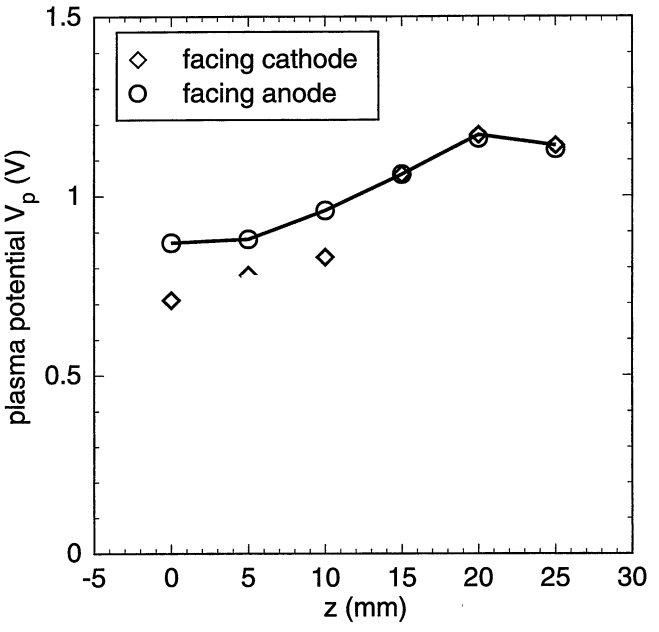

Fig. 3. Radial dependence of the plasma potential V_p (solid line) at $z=25$ mm. The plasma potential is taken as the more positive of the inflection points of the two planar probe characteristics measured at each radius. At $r=0$, 5 and 10 mm the inflection point of the cathode-facing characteristic is below that of the anode-facing characteristic, indicating a strong electron drift from the cathode to the anode.

interpolated by fitting[24] a shifted Maxwellian

$$g(v_z) \propto \exp\left[-\frac{1}{2} m(v_z - v_0)^2 / T_{\text{fit}}\right] \qquad (10)$$

to points in the neighborhood of $v_z = 0$. Here v_0 is a drift velocity, and T_{fit} is an electron temperature given in energy units. This fitted curve was used to compute moments of the distribution function near $v_z = 0$, as well as to estimate the density and temperature of the cold electron component at large radii.

The measured reduced electron distribution functions $g(v_z)$ are exhibited in Fig. 4. Here electrons with positive velocities are moving away from the cathode (to the anode), and those with negative velocities are moving toward the cathode (see Fig. 1). We plot $g(v_z)$ on a logarithmic scale to bring out detail in the tails. Here $g(v_z)$ decays rapidly for $|v_z| \gtrsim 1.8 \times 10^6$ m/s. This in not unexpected given that the inelastic (excitation) scattering threshold in Ar is 11.6 eV (2.0×10^6 m/s).

The distribution functions at $r = 0$, 5 and 10 mm exhibit a strong asymmetry, representing a net electron drift from the cathode to the anode. These distribution functions peak at $v_z > 0$, and have a deficit of negative-velocity electrons. As the plasma potential is positive (Fig. 3) the anode sheath represents a potential hill that electrons must climb to escape from the plasma. At the anode the more energetic electrons are lost, while the less energetic electrons are reflected. Consequently, it is reasonable to expect that there will be relatively few high energy electrons with negative velocities. From the measured distribution functions we find that electrons with $v_z < 7 \times 10^5$ m/s are confined, so that the size of the potential barrier is ≈ 1.4 V, which is not too different from the measured plasma potential. The distribution function at $r = 15$ mm represents a transition between the $r = 0$, 5 and 10 mm distribution functions and the nearly symmetric distribution functions at $r = 20$ and 25 mm.

At $r = 20$ and 25 mm we see that $g(v_z)$ is nearly symmetric, and is characterized by two electron populations. There is a cold, ($T \approx 0.3$ eV) background Maxwellian component of electrons trapped in the potential well, and an approximately rectangular tail component. Such rectangular tails have been found in filament discharges, and are associated with shell distribution functions,[25,26] i.e., a mono-energetic population of electrons with an isotropic velocity distribution. The width of this rectangular tail is $\approx \pm 1.8 \times 10^6$ m/s (9.2 eV) at $r = 20$ mm and $\approx \pm 1.5 \times 10^6$ m/s (6.4 eV) at $r = 25$ mm. As discussed above, the electron distribution function should contain few electrons above the inelastic scattering threshold for Ar (2.0×10^6 m/s). Further, the elastic scattering cross-section for Ar is largest for electron energies of ≈ 10 eV (1.9×10^6 m/s). Because of the peak in the cross-section near 10 eV and the cut-off above 11.6 eV, most scattered electrons should have nearly the same energy, leading to a shell distribution function.

The electron density n [eq. (5)] found by integrating the reduced distribution functions is displayed in Fig. 5(a). The density is strongly peaked on axis, with a value $n = 5.9 \times 10^{15}$ m^{-3} at $r = 0$ mm. At larger radii the electron density is due primarily to the cold, background component. At $r = 20$ mm, 4.7% of the electrons are in the tails, and the proportion of energetic electrons declines for increasing radii to only 2.1% at $r = 25$ mm.

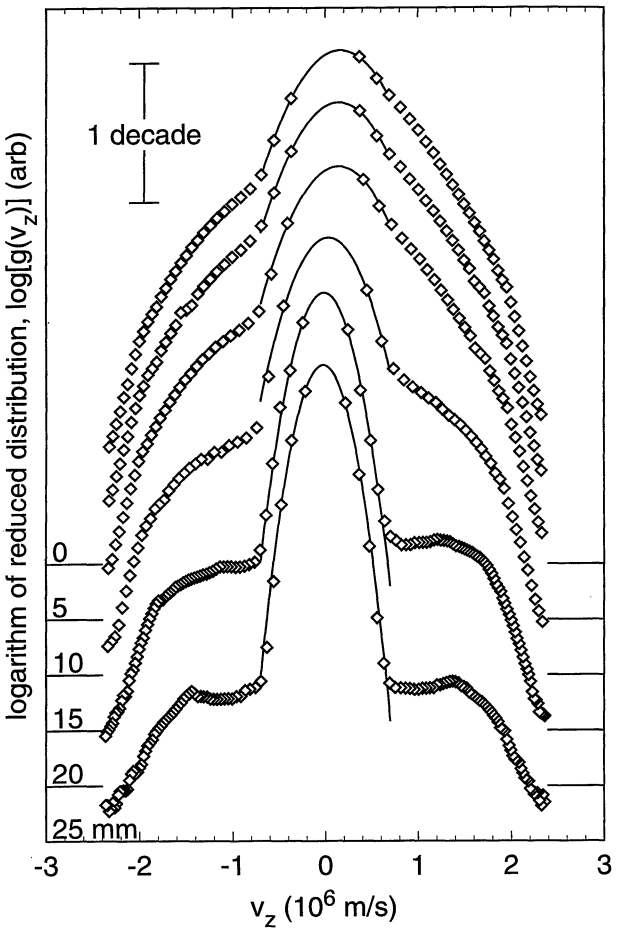

Fig. 4. Reduced distribution functions $g(v_z)$ taken at $r = 0$, 5, 10, 15, 20, and 25 mm ($r = 0$ mm is the topmost distribution function). Note that the vertical axis is logarithmic (the bar in the upper left hand corner is one decade tall), to emphasize the tails of the distribution functions. The baselines of the distribution functions are indicated. For $r = 0$, 5 and 10 mm the distribution functions are decidedly asymmetric with a net flux of electrons away from the cathode. At $r = 20$ and 25 mm the distribution functions are nearly symmetric and contain a cold Maxwellian component and an energetic tail component.

The average z-component of the electron velocity $\langle v_z \rangle$ [eq. (6)] is shown in Fig. 5(b). The average velocity is nearly constant for $r = 0$, 5 and 10 mm, with an average value of 1.9×10^5 m/s (0.10 eV), and then falls precipitously. The slight asymmetry in $g(v_z)$ at $r = 15$ mm gives $\langle v_z \rangle = 0.81 \times 10^5$ m/s (0.02 eV), 43% of the on-axis value. At $r = 20$ and 25 mm the average velocity acquires a (very) small negative value. At $r = 25$ mm, $\langle v_z \rangle = -0.21 \times 10^5$ m/s about 10% of the on-axis value. Note that $\langle v_z \rangle = -0.21 \times 10^5$ m/s (≈ 0.001 eV) is not distinguishable from $\langle v_z \rangle = 0$ in this experiment. The small values of $\langle v_z \rangle$ at $r = 20$ and 25 mm simply reflect the symmetry of the distribution function—the number of electrons with positive and negative veloci-

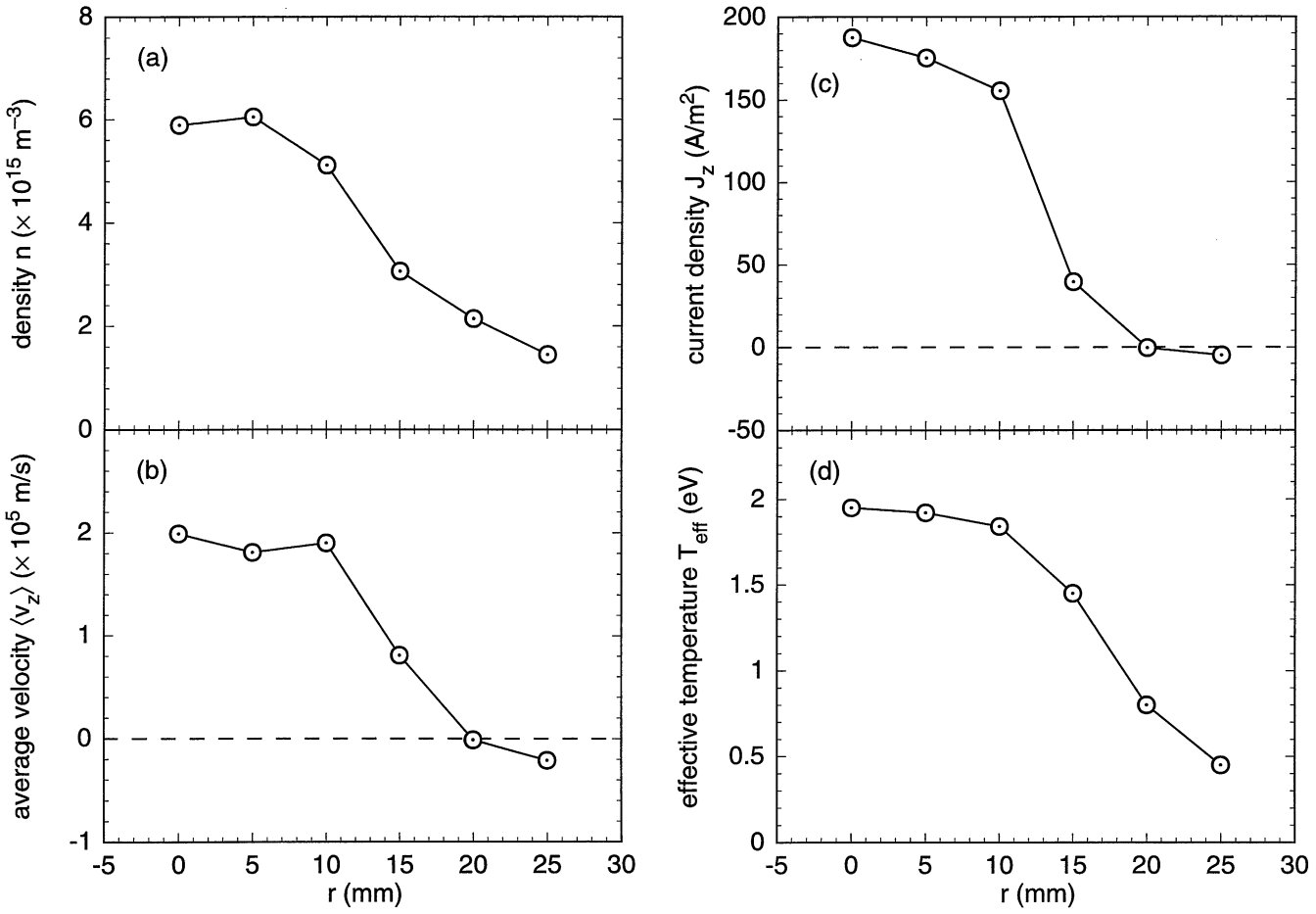

Fig. 5. Radial dependence of the (a) electron density n, (b) average z-component of the the electron velocity $\langle v_z \rangle$, (c) electron current density J_z and (d) effective electron temperature T_{eff}. These quantities were computed from the reduced distribution functions shown in Fig. 4. All quantities are peaked near the axis (the main electron flow) and decrease at larger radii. In particular, the current density is large for $r \leq 15$ mm, indicating a strong electron flow from the cathode to the anode.

ties are nearly equal.

The z-component of the electron current density J_z [eq. (7)] is strongly peaked on axis, as shown in Fig. 5(c), providing direct, unambiguous evidence for electron transport from the cathode to the anode. The peak value of the current density is 187 A/m^2. The strong on-axis current agrees with qualitative results of the Monte Carlo simulation reported in ref. 4 (in particular, see Fig. 7). At $r=20$ and 25 mm the current density is small and negative, representing a return current of electrons to the anode shield surrounding the magnetron. When J_z is integrated over radius we find 97.4 mA of total current, in comparison to the 51 mA of discharge current. The integrated current may be larger than the discharge current because we have not included the negative current density from radii larger than 25 mm. Even though for $r>25$ mm the current density is small, the area is large because of the cylindrical geometry.

The effective electron temperature [eq. (9)] decreases with increasing radius, as shown in Fig. 5(d). For $r=0$, 5 and 10 mm, T_{eff} is nearly constant with an average value 1.9 eV. At larger radii T_{eff} decreases as the proportion of energetic tail electrons declines. At $r=20$ mm, the effective temperature is 0.80 eV and at $r=25$ mm the effective temperature falls to 0.45 eV. For comparison, the temperatures of the cold component found from the fitted Maxwellian [eq. (10)] are 0.30 eV and 0.25 eV, respectively, (with an uncertainty of about ± 0.03 eV). These temperatures are in good agreement with those typically found (ignoring the tails) from cylindrical probe characteristics at these locations.

5. Conclusions

A consistent picture of electron transport in a sputtering magnetron discharge emerges from the detailed measurements of the electron distribution function presented here. Through some mechanism, either turbulence or more likely collisions with neutrals,[4,12] confined electrons are scattered out of the magnetic trap and on to unconfined orbits that reach the anode.[4] Because of the specific magnetic geometry of our device, electrons are funneled into a small region, $r \leq 15$ mm, around the cylindrical axis. The qualitative agreement of these results with those seen in Monte Carlo simulations[4] enhances our confidence that such simulations capture some of the important physics of electron transport in sputtering magnetrons. At the anode, the more energetic electrons overcome the

plasma sheath and escape from the plasma. Less energetic electrons are reflected by the sheath and form a population of electrons traveling back toward the cathode. These cold electrons are needed to balance the positive ion space charge. At larger radii, the distribution function consists almost entirely of cold electrons caught in the potential well. A few percent of the electrons are, however, found to be in rectangular tails, indicating a shell-like distribution function. We speculate that these are energetic electrons scattered out of the main flow by electron-neutral collisions.

Acknowledgment

This work was supported by the Iowa Department of Economic Development and National Science Foundation grant ECS-92-15882.

1) J. A. Thornton: J. Vac. Sci. & Technol. **15** (1978) 171.
2) R. K. Waits: J. Vac. Sci. & Technol. **15** (1978) 179.
3) A. E. Wendt, M. A. Lieberman and H. Meuth: J. Vac. Sci. & Technol. A **6** (1988) 1827.
4) T. E. Sheridan, M. J. Goeckner and J. Goree: J. Vac. Sci. & Technol. A **8** (1990) 30.
5) J. E. Miranda, M. J. Goeckner, J. Goree and T. E. Sheridan: J. Vac. Sci. & Technol. A **8** (1990) 1627.
6) S. Ido and K. Nakamura: Jpn. J. Appl. Phys. **32** (1993) 5698.
7) E. Shidoji, M. Nemoto, T. Nomura and Y. Yoshikwa: Jpn. J. Appl. Phys. **33** (1994) 4281.
8) T. E. Sheridan, M. J. Goeckner and J. Goree: Appl. Phys. Lett. **57** (1990) 2080.
9) J. Goree and T. E. Sheridan: Appl. Phys. Lett. **59** (1991) 1052.
10) S. M. Rossnagel and H. R. Kaufmann: J. Vac. Sci. & Technol. A **4** (1986) 1822.
11) B. C. Bell and D. A. Glocker: J. Vac. Sci. & Technol. A **6** (1988) 2047.
12) T. E. Sheridan and J. Goree: J. Vac. Sci. & Technol. A **7** (1989) 1014.
13) I. Petrov, I. Ivanov, V. Orlinov and J. Kourtev: Contrib. Plasma Phys. **30** (1990) 223.
14) M. J. Goeckner, J. Goree and T. E. Sheridan: J. Vac. Sci. & Technol. A **8** (1990) 3920.
15) M. J. Goeckner, J. Goree and T. E. Sheridan: IEEE Trans. Plasma Sci. **19** (1991) 301.
16) L. Gu and M. A. Lieberman: J. Vac. Sci. & Technol. A **6** (1988) 2960.
17) S. Miyake, N. Shimura, T. Makabe and A. Itoh: J. Vac. Sci. & Technol. A **10** (1992) 1135.
18) T. E. Sheridan, M. J. Goeckner, and J. Goree: J. Vac. Sci. & Technol. A **9** (1991) 688.
19) S. M. Rossnagel and H. R. Kaufmann: J. Vac. Sci. & Technol. A **5** (1987) 88.
20) T. E. Sheridan, M. J. Goeckner and J. Goree: J. Vac. Sci. & Technol. A **8** (1990) 1623.
21) T. E. Sheridan and J. Goree: Phys. Rev. E **50** (1994) 2991.
22) W. Gekelman and R. L. Stenzel: Phys. Fluids **21** (1978) 2014.
23) B. Windows and N. Savvides: J. Vac. Sci. & Technol A **4** (1986) 196.
24) W. H. Press, B. P. Flannery, S. A. Teukolsky and W. T. Vetterling: *Numerical Recipes in C* (Cambridge University Press, Cambridge, 1988) p. 540.
25) N. Hershkowitz, J. R. DeKock, P. Coakley and S. L. Cartier: Rev. Sci. Instrum. **51** (1980) 64.
26) N. Hershkowitz, R. L. Goettsch, C. Chan, K. Hendriks and R. T. Carpenter: J. Appl. Phys. **53** (1982) 5330.